

Article

Immobilization of Graphene Oxide on the Permeate Side of a Membrane Distillation Membrane to Enhance Flux

Worawit Intrchom, Sagar Roy , Madihah Saud Humoud and Somenath Mitra *

Department of Chemistry and Environmental Science, New Jersey Institute of Technology, Newark, NJ 07102, USA; wi6@njit.edu (W.I.); sagar@njit.edu (S.R.); msh36@njit.edu (M.S.H.)

* Correspondence: somenath.mitra@njit.edu; Tel.: +1-973-596-5611; Fax: +1-973-596-3586

Received: 13 July 2018; Accepted: 13 August 2018; Published: 15 August 2018



Abstract: In this paper, a facile fabrication of enhanced direct contact membrane distillation membrane via immobilization of the hydrophilic graphene oxide (GO) on the permeate side (GOIM-P) of a commercial polypropylene supported polytetrafluoroethylene (PTFE) membrane is presented. The permeate side hydrophilicity of the membrane was modified by immobilizing the GO to facilitate fast condensation and the withdrawal of the permeate water vapors. The water vapor flux was found to be as high as 64.5 kg/m²·h at 80 °C, which is 15% higher than the unmodified membrane at a feed salt concentration of 10,000 ppm. The mass transfer coefficient was observed 6.2 × 10⁻⁷ kg/m²·s·Pa at 60 °C and 200 mL/min flow rate in the GOIM-P.

Keywords: graphene oxide; membrane distillation; flux; desalination; mass transfer coefficient

1. Introduction

The demand for clean water has considerably increased around the world and is becoming a critical issue due to an increasing population and growing industrialization [1]. The consumption in industrial sector alone was up by more than 200% in 2015 when compared to 1995 [2]. The amount of freshwater in the world is limited and much of it is polluted, and consequently brackish or sea water are attractive sources of pure water [3]. However, energy efficient and cost effective desalination processes are important for that to happen. There are two most popular techniques for desalination, namely reverse osmosis (RO) and multi-stage flash (MSF) distillation [4,5]. While these are well established techniques that have much merit, they face limitations, such as high energy consumption, fouling, and high capital investment [6]. As a result, alternative desalination technologies, including solar evaporation and membrane distillation (MD), are being explored [4,7].

In the MD process, a hot feed is used to generate a vapor pressure gradient across the porous hydrophobic membrane and the vapors are condensed in a cold permeate [8–10]. The process can be conducted at a relatively low temperature (50–90 °C), hence waste heat, solar energy, or geothermal energy can be utilized as heat sources for heating the brine [11–15]. Other advantages include high rejection of the dissolved non-volatile species, able to handle highly concentrated brine with less fouling, low operating pressure, and less space requirement when compared to MSF [8,16–18]. However, MD still is faced with some barriers, such as relatively low water vapor flux in comparison with other conventional systems, flux reduction due to temperature and concentration polarization, pore wetting and membrane fouling, and lack of high-efficiency membranes [19,20].

Several hydrophobic polymers, including polytetrafluoroethylene (PTFE), polypropylene (PP), and polyvinylidene difluoride (PVDF) have been utilized as membrane materials [9,21–23], and different methods have been employed for the synthesis and modification of these membranes to

improve the performances [24–36]. Nanotechnology has enabled the development of advanced membranes based separation techniques [18,24,26,29,31–35,37–39]. Nanomaterials (NMs), such as Fe_3O_4 , TiO_2 , SiO_2 , carbon nanotubes (CNTs), nanodiamonds (NDs), and graphene oxide (GO) have been incorporated via blending or coating method to improve the membrane efficiency [10,18,24,32–35,39–42], and different functionalized CNTs were used to fabricate a bilayered structures that have shown significant enhancement in flux [32]. Recently, GO has found a niche in membrane separations [43,44]. The GO is comprised of highly oxidized graphene sheet having various functional groups, including hydroxyl, carbonyl, and epoxy groups on its surface. These functional groups minimize the aggregation of GO in dispersion state, provide reaction moieties and make GO hydrophilic [45]. Recent studies have shown that GO could potentially improve the mechanical properties as well as selectivity, antifouling, and the permeate flux [33,46–48].

In MD, membrane itself plays the crucial role in enhancing the flux and selectivity. While most of the researches have focused on different membrane modifications [24,27,28,30,33,48], our previous studies have shown that permeate side hydrophilization of the membrane can significantly improve the water vapor permeation rate [16]. The rapid water vapor removal from the permeate side boundary layer is one of the most important consideration in increasing the concentration gradient for enhanced mass transfer. However, hydrophilization using strong oxidizing agents are quite hazardous and tend to reduce the mechanical strength of the membrane. An approach that involves NM modification by immobilizing hydrophilic NMs has the advantage of improving membrane characteristics as well as easy adjustment. GO can be significantly hydrophilic with high oxygen content and it is conceivable that the hydrophilicity of the permeate side can be improved by the incorporation of GO. In our previous study, the immobilization of the GO in the feed side have shown significant enhancement in flux [42]. There, the GO was instrumental in enhancing the partition coefficient and permeation of water vapor from the feed side. In the present study, we present a complimentary approach where the GO is immobilized on the permeate side. Here, the GO enhances the overall flux by providing sites for condensation of the permeated water vapor, which facilitates the rapid removal of water, thus enhancing overall mass transport.

2. Materials and Methods

2.1. Materials

Sodium chloride (NaCl), acetone, GO sheet (42–52% carbon), and polyvinylidene difluoride (PVDF) powder (Mw ~500 K) were purchased from Sigma–Aldrich (St. Louis, MO, USA). Deionized water was used in all experiments. The membrane that was used in the MD experiments was flat composite PTFE membrane supported with polypropylene nonwoven fabric (Advantec MFS, Dublin, CA, USA; 129 μm thick, 0.2 μm pore size and 70% porosity).

2.2. Experimental Procedure

MD experiments were conducted in the direct contact MD (DCMD) configuration. Figure 1 shows the schematic diagram of the MD system used in the laboratory. The system consists of a DCMD cell and PTFE membrane with an effective contact area of 11.94 cm^2 . The feed and permeate flow were regulated by peristaltic pumps (MasterFlex Easy Load, Cole-Parmer, Vernon, IL, USA). The hot aqueous NaCl solution at different concentrations was passed through the feed side of the membrane in the DCMD cell and the cold distilled water was pumped through the permeate side of the membrane. Additional hot water was supplied to the feed water reservoir throughout the experiment to maintain the concentration constant. A counter current flow mode was used for feed and permeate water flow through the module. The constant temperature water bath (Neslab Water Bath Model GP 200, NESLAB Instruments, Inc., Newington, NH, USA) was used to maintain constant feed temperature, and the permeate temperature around 18 $^\circ\text{C}$ was controlled by a bench top chiller (Polyscience LS5, Cole-Parmer, USA). Temperatures of feed and permeate side were monitored by temperature sensors

(Four-channel Data Logging Thermometer, RS-232, Cole-Parmer, USA). The experiment was repeated for three times and less than 1% relative standard deviation was observed.

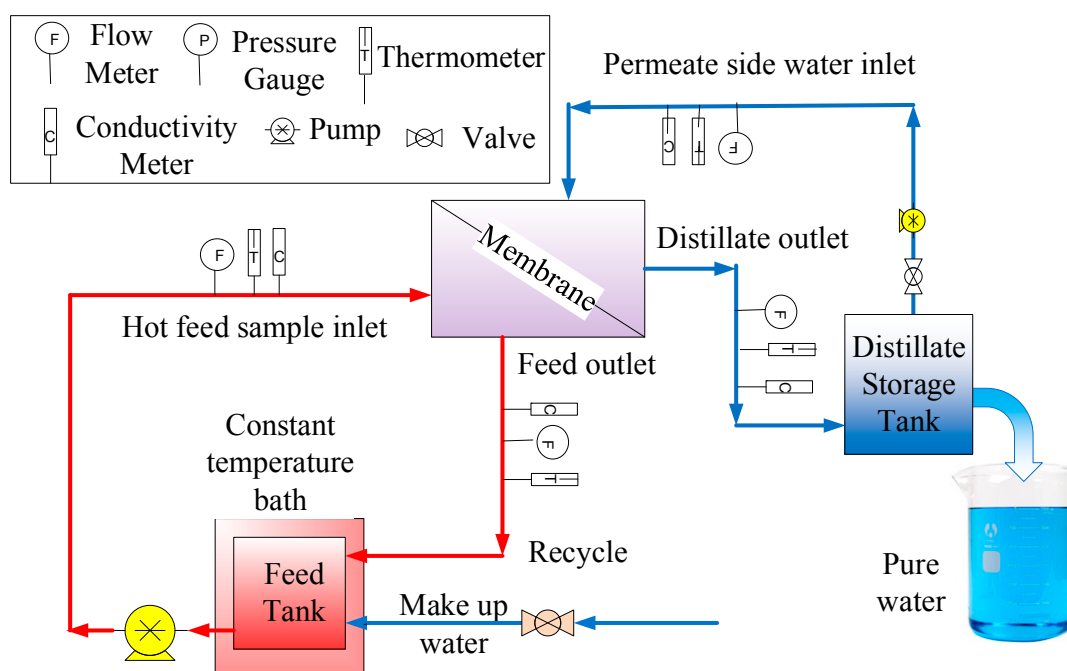


Figure 1. Schematic diagram of the experimental set up for direct contact membrane distillation (DCMD) application.

2.3. Fabrication of GOIM-P

In fabrication of the graphene oxide immobilized membrane on the permeate side (GOIM-P), the uniform dispersion of GO in the organic solvent and immobilization of GO on the membrane surfaces are considered the most important steps during membrane fabrication. Ten mg of GO was added to 8 g of acetone and sonicated for 10 h to ensure the uniform dispersal of GO into the organic solvent. 0.2 mg of PVDF was separately dissolved in 2 g of acetone and the PVDF solution was finally mixed with GO suspension. The mixed PVDF-GO suspension was then cast drop wise slowly and uniformly on the permeate side of the membrane to immobilize the GO on the surface. After that, the immobilized membrane was rinsed with extra acetone to remove excess PVDF from the membrane pores and the surface.

2.4. Characterization of GOIM-P

A scanning electron microscopy (SEM, Model LEO 1530, Carl Zeiss SMT AG Company, Oberkochen, Germany) was used to characterize the morphology of the fabricated GOIM-P. The samples for SEM was prepared by cutting the membranes into a square of 0.5 cm × 0.5 cm, placing on a specimen stub followed by carbon coating. The GOIM-P was further illustrated by Raman spectroscopy (DXR Raman microscope, Thermo Scientific, Waltham, MA, USA). The thermal stability of GOIM-P was investigated by thermal gravitational analysis (TGA 8000, Thermogravimetric analyzer, PerkinElmer, Waltham, MA, USA). The contact angles measurements were used to study the hydrophobicity/hydrophilicity of the permeate surface while using an Attension apparatus (model Theta, Biolin Scientific UK, Manchester, UK). The water drop method on dry membrane was employed and five measurements were taken to obtain the average value.

3. Results and Discussion

3.1. Characterization of GOIM-P

Figure 2a–c show the SEM images of the unmodified PTFE membrane (feed side and permeate side), and GOIM-P (permeate side), respectively. Figure 2a clarifies the presence of active pores on the membrane feed surface. While Figure 2c demonstrates the change in morphology from Figure 2b due to the immobilization of the GO on the permeate surface.

Raman spectra of the GOIM-P are shown in Figure 3. Prominent Raman peaks of support polypropylene layer on the permeate side of the composite membrane were observed at 800, 1500, 2700, and 3000 cm^{-1} [49]. The presence of GO on the membrane is shown at 1349 cm^{-1} that could be ascribed to the graphite defect in the sp^3 domain via oxidation and an additional peak at 1597 cm^{-1} is due to stretching mode of graphite [50].

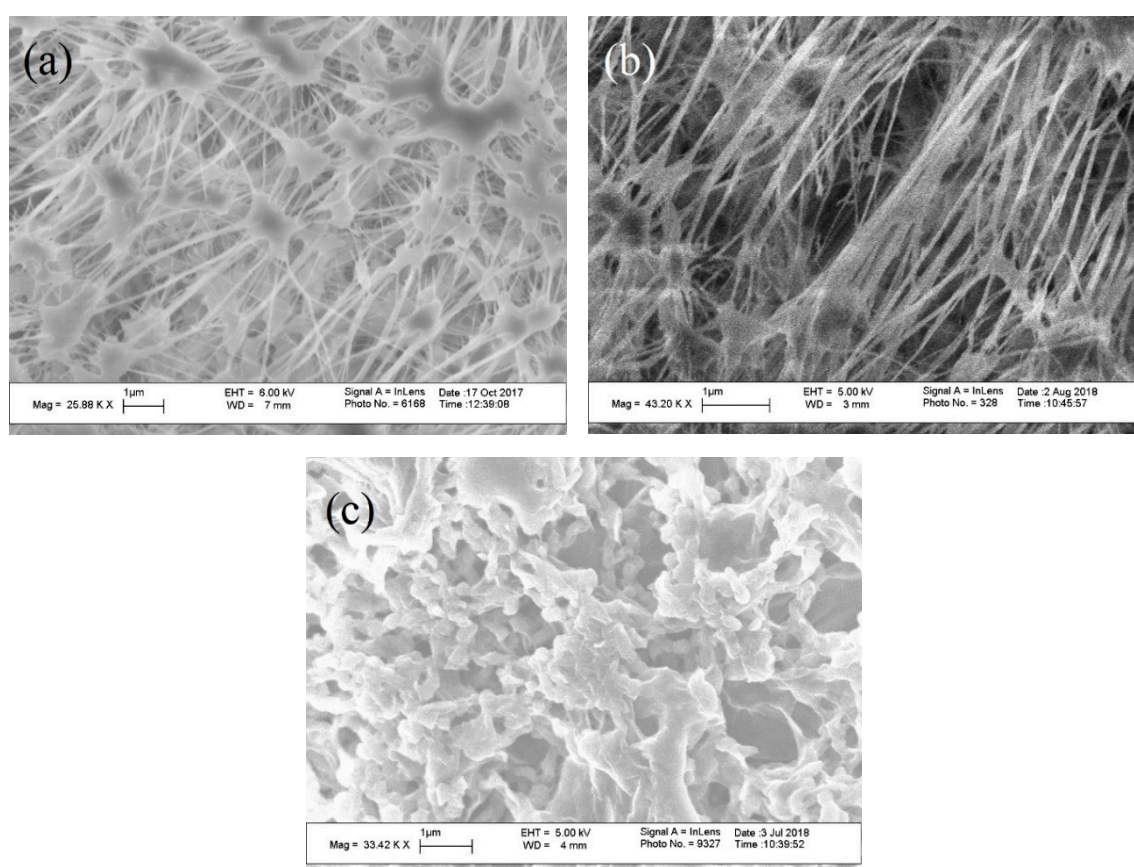


Figure 2. Scanning electron micrographs of (a) feed side and (b) permeate side of the unmodified polytetrafluoroethylene (PTFE) membrane; and, (c) graphene oxide immobilized membrane on the permeate side (GOIM-P) (permeate side).

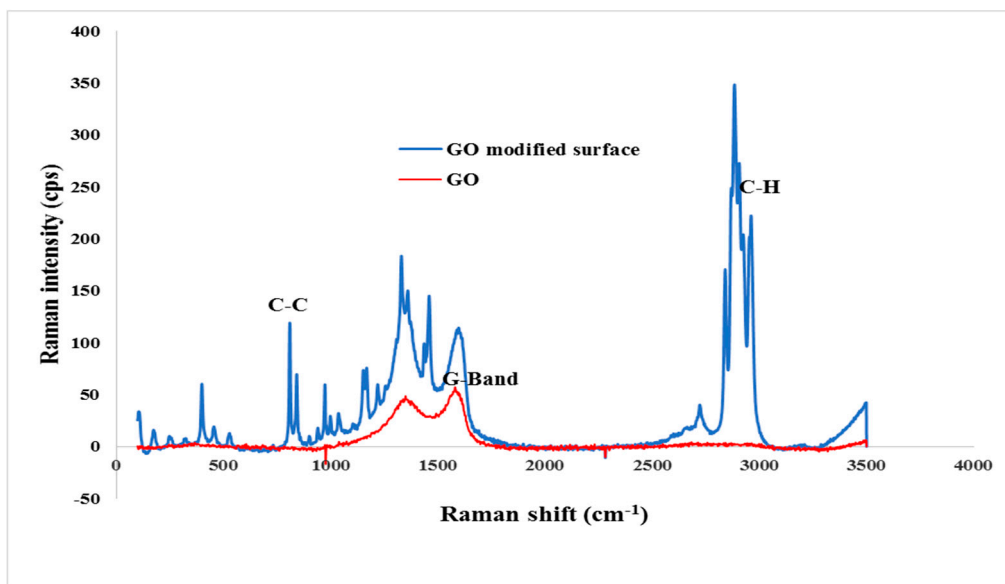


Figure 3. Raman spectra of the permeate surface of GOIM-P.

The thermal stability is an important parameter for membranes used in MD as the membranes must resist with high temperature salt solution. In this study, TGA curves were used to evaluate the stability of GOIM-P in comparison with unmodified membrane, as shown in Figure 4. The weight loss at around 230 °C to 330 °C was due to the decomposition of PP as the supporting layer, while PTFE began to decompose at around 460–470 °C. It was observed that the presence of GO provided additional thermal stability of the modified membrane. Increasing in the thermal stability of GOIM-P could be due to GO particles and the functional groups on GO that play the role as a reducing and sacrificed agent that lead to slow down or limit the degradation process [51]. The result is in line with what we have reported previously [32,36].

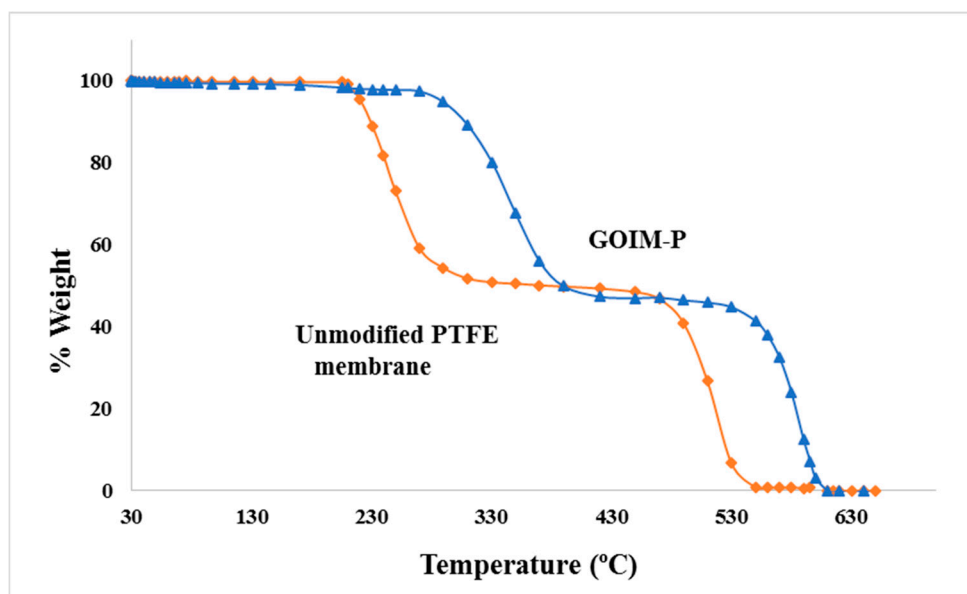


Figure 4. Thermal gravitational analysis (TGA) curves of unmodified and GOIM-P.

The hydrophobicity on the permeate surface of GOIM-P was determined by contact angle analysis. After GO immobilization, the contact angle on the permeate side of the modified membrane showed a

decrease from $94^\circ \pm 2^\circ$ to $75^\circ \pm 2^\circ$. A decreasing of contact angle implied that the hydrophilicity on the permeate side of the GOIM-P increases by increasing the surface energy and this was expected to enhance the membrane performances. The contact angle values and photographs of permeate side of unmodified and GOIM-P are shown in Figure 5.

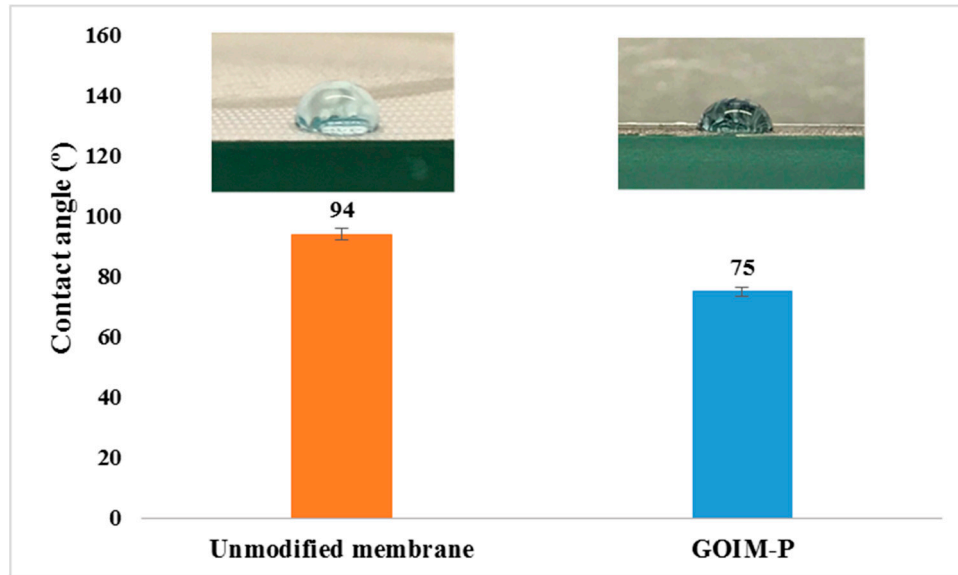


Figure 5. Contact angle and photographs of permeate side of unmodified and GOIM-P.

3.2. DCMD Performance of GOIM-P

The overall permeate flux, J_w , is expressed as:

$$J_w = \frac{W_p}{t \cdot A} \quad (1)$$

where, W_p is the total mass collected from the permeate side, t is the run time, and A is the effective membrane area. Temperature, feed flow rate, and salt concentration were varied in the experiment to evaluate the performance of the GOIM-P, and of the unmodified membrane.

3.2.1. Effect of Temperature and Feed Flow Rate on Water Vapor Flux

The effect of temperature on permeate flux of the GOIM-P when compared to the pristine membrane is illustrated in Figure 6a. It is clear from the figure that the fluxes significantly increased with increase in temperature for both membranes. Increasing in vapor pressure with temperature plays the major role in flux increment [52]. It is clearly seen that the GOIM-P produced a higher amount of permeated water when compared to the pristine membrane. Maximum permeate flux was $64.5 \text{ kg/m}^2 \cdot \text{h}$ at feed temperature of 80°C , which is 15% higher as compared to the pristine membrane.

The influence of increasing feed flow rate at a constant temperature of 60°C and 200 mL/min permeate flow rate is displayed in Figure 6b. It was observed that the permeate flux increased with an increase in feed flow rate in both membranes and the GOIM-P offered higher water vapor flux when compared to the unmodified one. The increased feed flow rate enhances the turbulence and reduces the boundary layer effect at the membrane-feed solution interface. These result in the reduction of temperature polarization and improving the permeate flux [53,54].

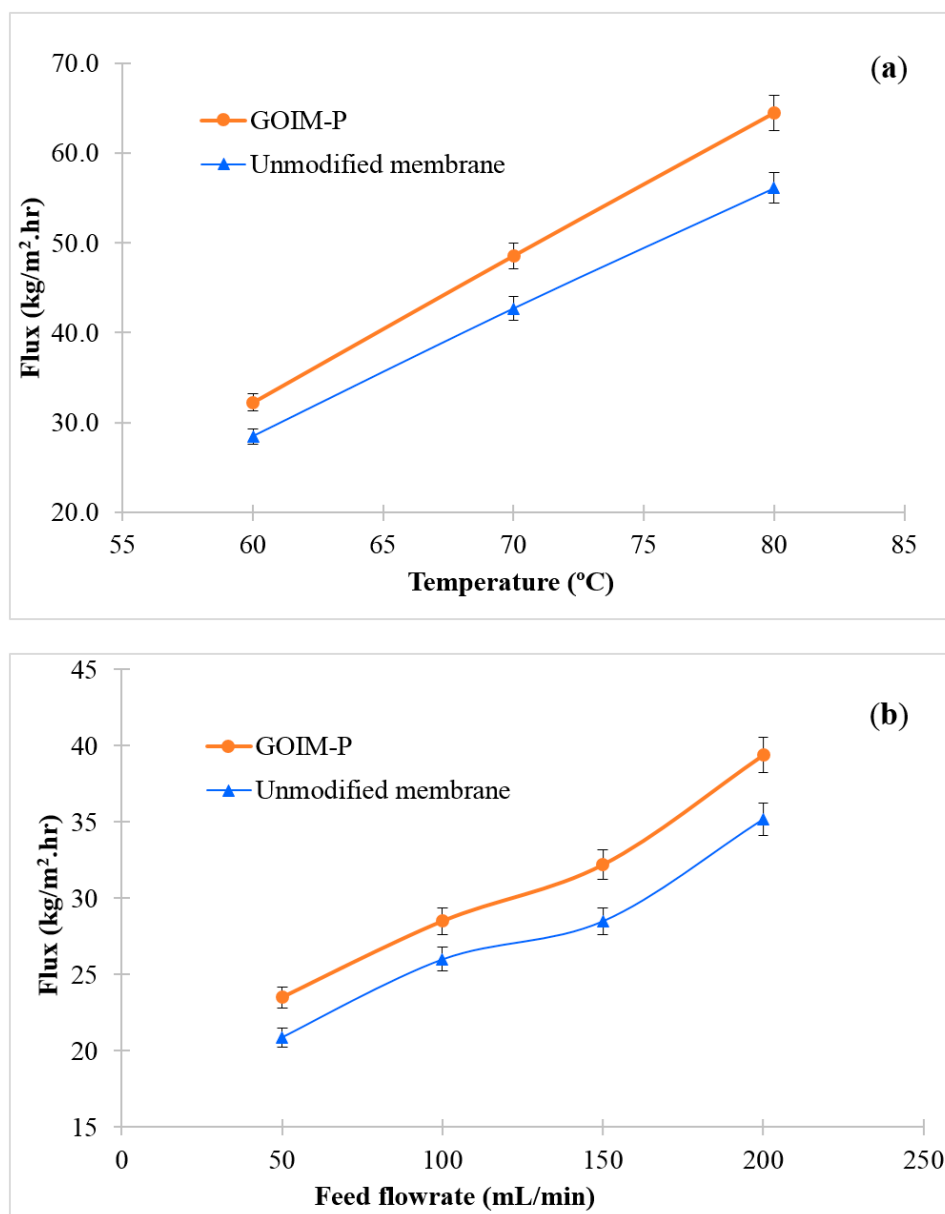


Figure 6. Effect of (a) temperature on water vapor flux at a feed flow rate of 150 mL/min; and, (b) feed flow rate on water vapor flux at feed temperature of 60 °C.

3.2.2. Effect of Salt Concentration

Figure 7 shows the effect of varying salt concentrations in feed solution on permeate flux. With increase in concentration, both membranes show a decrease in water vapor flux as expected. The increase in feed salt concentration led to the reduction of the water activity at the membrane-solution interface and the formation of additional boundary layer directly affect the driving force across the membrane and reduces the water vapor flux. Similar results have been reported before [55,56]. As a result of increasing salt concentration from 3400 to 34,000 ppm, the permeate flux reduced from 29.7 to 24.3 kg/m²·h, and 33.9 to 26.8 kg/m²·h for the unmodified membrane and GOIM-P, respectively. The conductivity of the permeated water did not change with varying salt concentrations, indicating the complete rejection of the salt.

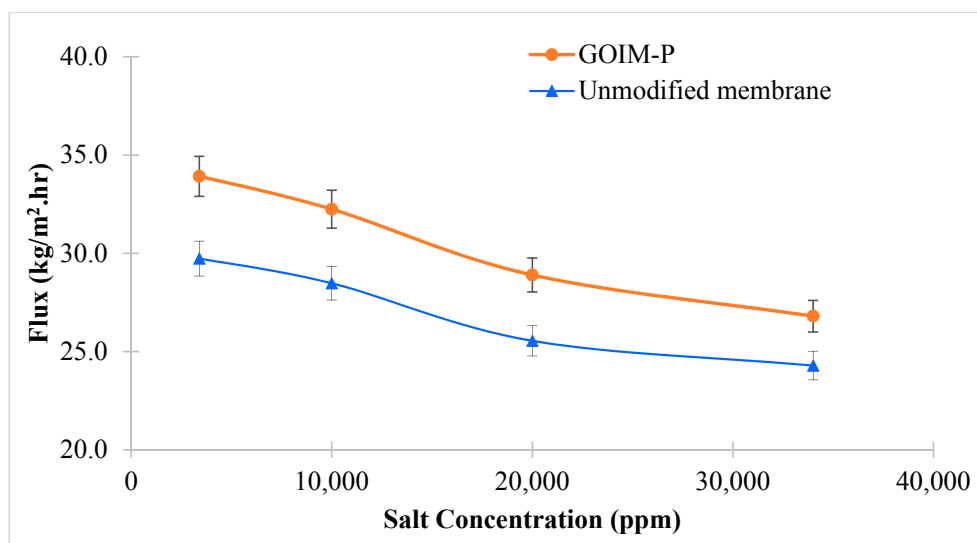


Figure 7. Effect of varying feed concentration on water vapor flux at feed flow rate of 150 mL/min and operating temperature of 60 °C.

3.2.3. Mass Transfer Coefficient

The overall, mass transfer coefficient can be described as:

$$J_w = k(P_f - P_p)$$

$$\text{or, } k = \frac{J_w}{(P_f - P_p)} \tag{2}$$

where, J_w is the water vapor flux, k is mass transfer coefficient, and P_f and P_p are partial vapor pressure of average feed and permeate temperatures. The mass transfer coefficients were found to be higher for GOIM-P as compared to the unmodified membrane.

Table 1 summarizes the change in mass transfer coefficients of GOIM-P and the unmodified membrane with varying feed flow rate at 60 °C. Both membranes exhibited increased mass transfer coefficient with increase in feed flow rate. The diffusion of the water vapor through the boundary layers mainly controls the overall mass transfer rate of the process. At higher feed flow rate, the turbulence increased that led to the reduction in the boundary layer resistance and significantly increased the mass transfer coefficients. Among these two membranes, GOIM-P exhibited higher mass transfer coefficient in comparison with the pristine membrane.

Table 1. Effect of varying feed flow rate on mass transfer coefficient at 60 °C.

Feed Flow Rate (mL/min)	$k \text{ (kg/m}^2 \cdot \text{s} \cdot \text{Pa)} \times 10^{-7}$	
	Unmodified Membrane	GOIMP
50	3.3	3.7
100	4.1	4.5
150	4.5	5.1
200	5.56	6.2

3.3. Stability and Salt Breakthrough

The quality of permeate side water was carefully investigated to monitor the stability of modified membrane and salt breakthrough. The stability of GOIM-P was tested for a long period of operation, as shown in Figure 8. The permeated water was monitored throughout the experiment to ensure

the quality of water by measuring the conductivity of the permeate side water and using Raman spectroscopy [43,57]. The results did not show any leakage of salt through the membrane and the presence of GO in the permeate water samples.

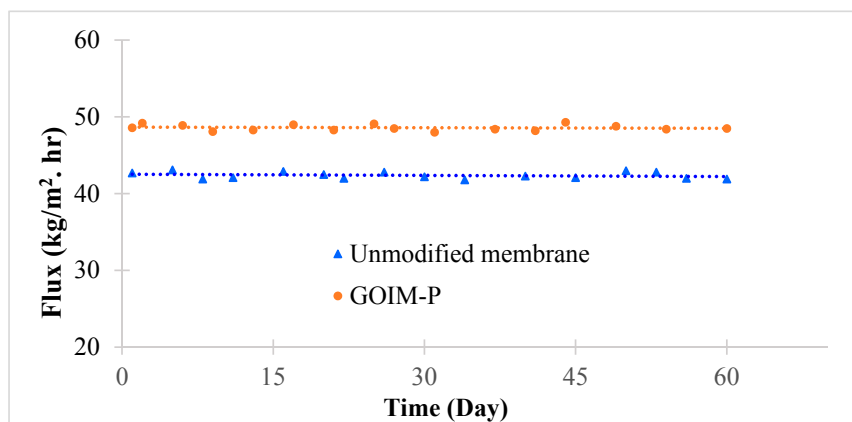


Figure 8. Stability of the membranes at a 70 °C feed temperature and 10,000 ppm of NaCl solution.

4. Proposed Mechanism

The proposed mechanism in GOIM-P is shown in Figure 9. A significant enhancement in water vapor flux was noticed with the inclusion of GO in the permeate side. The hydrophilicity of the membrane permeate side was enhanced due to the presence of polar epoxy and carboxyl and hydroxyl functional groups on GO that allow for the water vapor to interact with the modified permeate surface [58,59]. In MD, the water vapor permeation through the membrane is steered by the vapor pressure gradient present across the membrane. A boundary layer comprising probably of both liquid and vapor phases is formed on both side of the membrane. Although, the feed side layer remains unchanged in GOIM-P, the hydrophilic surface permitted fast water vapor removal, destabilization of vapor-gap, and mass transfer resistance reduction between the bulk permeate and membrane surface. These effects are equivalent to the contraction in permeate side boundary layer [16,60,61], which led to an enhancement in water vapor permeation through the membrane.

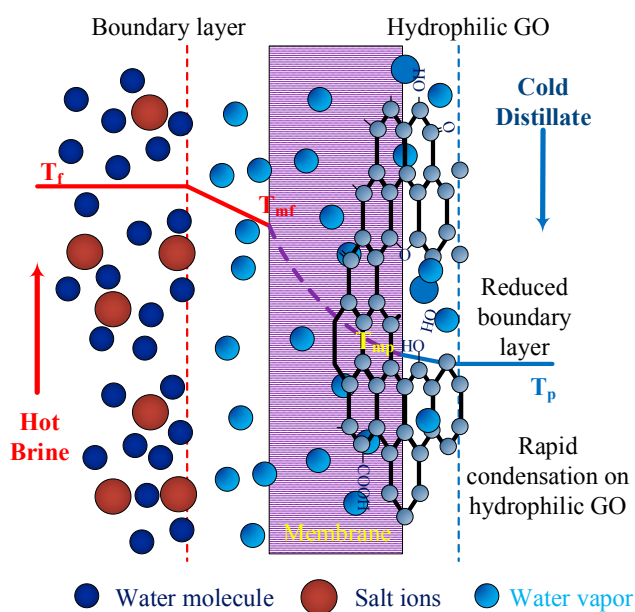


Figure 9. Proposed mechanism for GOIM-P.

5. Conclusions

GO was successfully immobilized on the permeate side of the PTFE membrane to increase the pure water flux in direct contact membrane distillation. It was evident that the introduction of hydrophilicity on the permeate side was effective in the rapid condensation and removal of the permeate, thus enhancing the mass transfer coefficient. The DCMD performance of GOIM-P was consistently superior compared to the pristine membrane and attaining a maximum water vapor flux of 64.5 kg/m²·h at 80 °C, which is 15% higher. The membrane was also found quite stable for a longer period of operation.

Author Contributions: S.M. and S.R. conceived and defined the problem. W.I., M.S.H. and S.R. developed the methodology and case studies. All of the authors contributed to the discussion. S.M. and S.R. supervised the experiments and technical writing, and reviewed and finalized the paper structure.

Funding: This study was partially supported by a grant from the Chemical, Bioengineering, Environmental, and Transport Systems Division, National Science Foundation (grant number CBET-1603314).

Conflicts of Interest: The authors declare no conflict of interest.

References

1. Curry, E. Water Scarcity and the Recognition of the Human Right to Safe Freshwater. *Hum. Rights* **2010**, *9*, 103.
2. Thorne, V.T.; Thomas, W.L. Issues of Water Scarcity and Rights for Multinational Companies. *Nat. Resour. Environ.* **2003**, *18*, 31–35.
3. Shirazi, M.M.A.; Kargari, A.; Shirazi, M.J.A. Direct contact membrane distillation for seawater desalination. *Desalin. Water Treat.* **2012**, *49*, 368–375. [[CrossRef](#)]
4. Khawaji, A.D.; Kutubkhanah, I.K.; Wie, J.-M. Advances in seawater desalination technologies. *Desalination* **2008**, *221*, 47–69. [[CrossRef](#)]
5. Nicolai, A.; Sumpster, B.G.; Meunier, V. Tunable water desalination across graphene oxide framework membranes. *Phys. Chem. Chem. Phys.* **2014**, *16*, 8646–8654. [[CrossRef](#)] [[PubMed](#)]
6. Wade, N.M. Distillation plant development and cost update. *Desalination* **2001**, *136*, 3–12. [[CrossRef](#)]
7. Roy, S.; Humoud, M.S.; Intrichom, W.; Mitra, S. Microwave-Induced Desalination via Direct Contact Membrane Distillation. *ACS Sustain. Chem. Eng.* **2017**, *6*, 626–632. [[CrossRef](#)]
8. Shirazi, A.; Mahdi, M.; Kargari, A. A Review on Applications of Membrane Distillation (MD) Process for Wastewater Treatment. *J. Membr. Sci. Res.* **2015**, *1*, 101–112.
9. Bhadra, M.; Roy, S.; Mitra, S. Flux enhancement in direct contact membrane distillation by implementing carbon nanotube immobilized PTFE membrane. *Sep. Purif. Technol.* **2016**, *161*, 136–143. [[CrossRef](#)]
10. Roy, S.; Bhadra, M.; Mitra, S. Enhanced desalination via functionalized carbon nanotube immobilized membrane in direct contact membrane distillation. *Sep. Purif. Technol.* **2014**, *136*, 58–65. [[CrossRef](#)]
11. Zhang, Y.; Sivakumar, M.; Yang, S.; Enever, K.; Ramezani-pour, M. Application of solar energy in water treatment processes: A review. *Desalination* **2018**, *428*, 116–145. [[CrossRef](#)]
12. Kabeel, A.; Abdelgaied, M.; El-Said, E.M. Study of a solar-driven membrane distillation system: Evaporative cooling effect on performance enhancement. *Renew. Energy* **2017**, *106*, 192–200. [[CrossRef](#)]
13. Shim, W.G.; He, K.; Gray, S.; Moon, I.S. Solar energy assisted direct contact membrane distillation (DCMD) process for seawater desalination. *Sep. Purif. Technol.* **2015**, *143*, 94–104. [[CrossRef](#)]
14. Dow, N.; Gray, S.; Zhang, J.; Ostarcevic, E.; Liubinas, A.; Atherton, P.; Duke, M. Pilot trial of membrane distillation driven by low grade waste heat: Membrane fouling and energy assessment. *Desalination* **2016**, *391*, 30–42. [[CrossRef](#)]
15. Lokare, O.R.; Tavakkoli, S.; Rodriguez, G.; Khanna, V.; Vidic, R.D. Integrating membrane distillation with waste heat from natural gas compressor stations for produced water treatment in Pennsylvania. *Desalination* **2017**, *413*, 144–153. [[CrossRef](#)]
16. Ragonath, S.; Roy, S.; Mitra, S. Selective hydrophilization of the permeate surface to enhance flux in membrane distillation. *Sep. Purif. Technol.* **2016**, *170*, 427–433. [[CrossRef](#)]
17. Drioli, E.; Ali, A.; Macedonio, F. Membrane distillation: Recent developments and perspectives. *Desalination* **2015**, *356*, 56–84. [[CrossRef](#)]

18. Bhadra, M.; Roy, S.; Mitra, S. Enhanced desalination using carboxylated carbon nanotube immobilized membranes. *Sep. Purif. Technol.* **2013**, *120*, 373–377. [[CrossRef](#)]
19. El-Bourawi, M.S.; Ding, Z.; Ma, R.; Khayet, M. A framework for better understanding membrane distillation separation process. *J. Membr. Sci.* **2006**, *285*, 4–29. [[CrossRef](#)]
20. Roy, S.; Rangunath, S.; Mitra, S. Effect of module configuration on the overall mass recovery in membrane distillation. *Desalin. Water Treat.* **2017**, *95*, 74–79. [[CrossRef](#)]
21. Daer, S.; Kharraz, J.; Giwa, A.; Hasan, S.W. Recent applications of nanomaterials in water desalination: A critical review and future opportunities. *Desalination* **2015**, *367*, 37–48. [[CrossRef](#)]
22. Lawson, K.W.; Lloyd, D.R. Membrane distillation. *J. Membr. Sci.* **1997**, *124*, 1–25. [[CrossRef](#)]
23. Alkudhiri, A.; Darwish, N.; Hilal, N. Membrane distillation: A comprehensive review. *Desalination* **2012**, *287*, 2–18. [[CrossRef](#)]
24. Agbaje, T.A.; Al-Gharabli, S.; Mavukkandy, M.O.; Kujawa, J.; Arafat, H.A. PVDF/magnetite blend membranes for enhanced flux and salt rejection in membrane distillation. *Desalination* **2018**, *436*, 69–80. [[CrossRef](#)]
25. Zheng, R.; Chen, Y.; Wang, J.; Song, J.; Li, X.M.; He, T. Preparation of omniphobic PVDF membrane with hierarchical structure for treating saline oily wastewater using direct contact membrane distillation. *J. Membr. Sci.* **2018**, *555*, 197–205. [[CrossRef](#)]
26. Li, K.; Hou, D.; Fu, C.; Wang, K.; Wang, J. Fabrication of PVDF nanofibrous hydrophobic composite membranes reinforced with fabric substrates via electrospinning for membrane distillation desalination. *J. Environ. Sci.* **2018**. [[CrossRef](#)]
27. Zhao, J.; Shi, L.; Loh, C.H.; Wang, R. Preparation of PVDF/PTFE hollow fiber membranes for direct contact membrane distillation via thermally induced phase separation method. *Desalination* **2018**, *430*, 86–97. [[CrossRef](#)]
28. Chen, Y.; Zheng, R.; Wang, J.; Liu, Y.; Wang, Y.; Li, X.M.; He, T. Laminated PTFE membranes to enhance the performance in direct contact membrane distillation for high salinity solution. *Desalination* **2017**, *424*, 140–148. [[CrossRef](#)]
29. Woo, Y.C.; Tijing, L.D.; Park, M.J.; Yao, M.; Choi, J.S.; Lee, S.; Shon, H.K. Electrospun dual-layer nonwoven membrane for desalination by air gap membrane distillation. *Desalination* **2017**, *403*, 187–198. [[CrossRef](#)]
30. Munirasu, S.; Banat, F.; Durrani, A.A.; Haija, M.A. Intrinsically superhydrophobic PVDF membrane by phase inversion for membrane distillation. *Desalination* **2017**, *417*, 77–86. [[CrossRef](#)]
31. Eykens, L.; De Sitter, K.; Dotremont, C.; Pinoy, L.; Van der Bruggen, B. Coating techniques for membrane distillation: An experimental assessment. *Sep. Purif. Technol.* **2018**, *193*, 38–48. [[CrossRef](#)]
32. Bhadra, M.; Roy, S.; Mitra, S. A Bilayered Structure Comprised of Functionalized Carbon Nanotubes for Desalination by Membrane Distillation. *ACS Appl. Mater. Interfaces* **2016**, *8*, 19507–19513. [[CrossRef](#)] [[PubMed](#)]
33. Leaper, S.; Abdel-Karim, A.; Faki, B.; Luque-Alled, J.M.; Alberto, M.; Vijayaraghavan, A.; Gorgojo, P. Flux-enhanced PVDF mixed matrix membranes incorporating APTS-functionalized graphene oxide for membrane distillation. *J. Membr. Sci.* **2018**, *554*, 309–323. [[CrossRef](#)]
34. Li, Y.; Dong, S.; Zhu, L. Preparation of novel poly(vinylidene fluoride)/TiO₂ photocatalysis membranes for use in direct contact membrane distillation. *J. Nanopart. Res.* **2018**, *20*, 63. [[CrossRef](#)]
35. Okiel, K.; El-Aassar, A.H.M.; Temraz, T.; El-Etriby, S.; Shawky, H.A. Performance assessment of synthesized CNT/polypropylene composite membrane distillation for oil field produced water desalination. *Desalin. Water Treat.* **2016**, *57*, 10995–11007. [[CrossRef](#)]
36. Rangunath, S.; Roy, S.; Mitra, S. Carbon nanotube immobilized membrane with controlled nanotube incorporation via phase inversion polymerization for membrane distillation based desalination. *Sep. Purif. Technol.* **2018**, *194*, 249–255. [[CrossRef](#)]
37. Roy, S.; Singha, N.R. Polymeric Nanocomposite Membranes for Next Generation Pervaporation Process: Strategies, Challenges and Future Prospects. *Membranes* **2017**, *7*, 53. [[CrossRef](#)] [[PubMed](#)]
38. Roy, S.; Hussain, C.M.; Mitra, S. Carbon nanotube-immobilized super-absorbent membrane for harvesting water from the atmosphere. *Environ. Sci. Water Res. Technol.* **2015**, *1*, 753–760. [[CrossRef](#)]
39. Roy, S.; Ntim, S.A.; Mitra, S.; Sirkar, K.K. Facile fabrication of superior nanofiltration membranes from interfacially polymerized CNT-polymer composites. *J. Membr. Sci.* **2011**, *375*, 81–87. [[CrossRef](#)]

40. Zhang, H.; Li, B.; Sun, D.; Miao, X.; Gu, Y. SiO₂-PDMS-PVDF hollow fiber membrane with high flux for vacuum membrane distillation. *Desalination* **2018**, *429*, 33–43. [[CrossRef](#)]
41. Bhadra, M.; Roy, S.; Mitra, S. Nanodiamond immobilized membranes for enhanced desalination via membrane distillation. *Desalination* **2014**, *341*, 115–119. [[CrossRef](#)]
42. Bhadra, M.; Roy, S.; Mitra, S. Desalination across a graphene oxide membrane via direct contact membrane distillation. *Desalination* **2016**, *378*, 37–43. [[CrossRef](#)]
43. Ma, J.; Ping, D.; Dong, X. Recent Developments of Graphene Oxide-Based Membranes: A Review. *Membranes* **2017**, *7*, 52.
44. Thebo, K.H.; Qian, X.; Zhang, Q.; Chen, L.; Cheng, H.M.; Ren, W. Highly stable graphene-oxide-based membranes with superior permeability. *Nat. Commun.* **2018**, *9*, 1486. [[CrossRef](#)] [[PubMed](#)]
45. Yoon, H.W.; Cho, Y.H.; Park, H.B. Graphene-based membranes: Status and prospects. *Philos. Trans. R. Soc. A* **2016**, *374*. [[CrossRef](#)] [[PubMed](#)]
46. Xu, Z.; Zhang, J.; Shan, M.; Li, Y.; Li, B.; Niu, J.; Qian, X. Organosilane-functionalized graphene oxide for enhanced antifouling and mechanical properties of polyvinylidene fluoride ultrafiltration membranes. *J. Membr. Sci.* **2014**, *458*, 1–13. [[CrossRef](#)]
47. Hegab, H.M.; Zou, L. Graphene oxide-assisted membranes: Fabrication and potential applications in desalination and water purification. *J. Membr. Sci.* **2015**, *484*, 95–106. [[CrossRef](#)]
48. Zahirifar, J.; Karimi-Sabet, J.; Moosavian, S.M.A.; Hadi, A.; Khadiv-Parsi, P. Fabrication of a novel octadecylamine functionalized graphene oxide/PVDF dual-layer flat sheet membrane for desalination via air gap membrane distillation. *Desalination* **2018**, *428*, 227–239. [[CrossRef](#)]
49. Ahmad, S.R.; Young, R.J.; Kinloch, I.A. Raman Spectra and Mechanical Properties of Graphene/Polypropylene Nanocomposites. *Int. J. Chem. Eng. Appl.* **2015**, *6*. [[CrossRef](#)]
50. Saito, R.; Hofmann, M.; Dresselhaus, G.; Jorio, A.; Dresselhaus, M.S. Raman spectroscopy of graphene and carbon nanotubes. *Adv. Phys.* **2011**, *60*, 413–550. [[CrossRef](#)]
51. Nguyen, B.D.; Ngo, T.K.; Bui, T.H.; Pham, D.K.; Dinh, X.L.; Nguyen, P.T. The impact of graphene oxide particles on viscosity stabilization for diluted polymer solutions using in enhanced oil recovery at HTHP offshore reservoirs. *Adv. Nat. Sci. Nanosci. Nanotechnol.* **2015**, *6*, 015012. [[CrossRef](#)]
52. Mengual, J.I.; Khayet, M.; Godino, M.P. Heat and mass transfer in vacuum membrane distillation. *Int. J. Heat Mass Transf.* **2004**, *47*, 865–875. [[CrossRef](#)]
53. Camacho, L.M.; Dumée, L.; Zhang, J.; Li, J.D.; Duke, M.; Gomez, J.; Gray, S. Advances in Membrane Distillation for Water Desalination and Purification Applications. *Water* **2013**, *5*, 94–196. [[CrossRef](#)]
54. Gryta, M. Concentration of NaCl solution by membrane distillation integrated with crystallization. *Sep. Sci. Technol.* **2002**, *37*, 3535–3558. [[CrossRef](#)]
55. Wirth, D.; Cabassud, C. Water desalination using membrane distillation: Comparison between inside/out and outside/in permeation. *Desalination* **2002**, *147*, 139–145. [[CrossRef](#)]
56. Cath, T.Y.; Adams, V.D.; Childress, A.E. Experimental study of desalination using direct contact membrane distillation: A new approach to flux enhancement. *J. Membr. Sci.* **2004**, *228*, 5–16. [[CrossRef](#)]
57. Krishnamoorthy, K.; Veerapandian, M.; Yun, K.; Kim, S.J. The chemical and structural analysis of graphene oxide with different degrees of oxidation. *Carbon* **2013**, *53*, 38–49. [[CrossRef](#)]
58. Xie, T.; Liu, C.; Zhang, X. Molecular dynamics simulation in the application of direct air dehumidification by electro dialysis method. *Procedia Eng.* **2017**, *205*, 116–122. [[CrossRef](#)]
59. Fletcher, A.J.; Uygur, Y.; Thomas, K.M. Role of surface functional groups in the adsorption kinetics of water vapor on microporous activated carbons. *J. Phys. Chem. C* **2007**, *111*, 8349–8359. [[CrossRef](#)]
60. Dumée, L.F.; Gray, S.; Duke, M.; Sears, K.; Schütz, J.; Finn, N. The role of membrane surface energy on direct contact membrane distillation performance. *Desalination* **2013**, *323*, 22–30. [[CrossRef](#)]
61. Khayet, M.; Mengual, J.; Matsuura, T. Porous hydrophobic/hydrophilic composite membranes: Application in desalination using direct contact membrane distillation. *J. Membr. Sci.* **2005**, *252*, 101–113. [[CrossRef](#)]

